A Converter-Based Hardware Testbed Hybrid Microgrid Emulator of a Flexible Manufacturing Plant

2023 IEEE Energy Conversion Congress and Exposition (ECCE) | 979-8-3503-1644-5/23/$31.00 ©2023 IEEE | DOI: 10.1109/ECCE53617.2023.10362111

Mohamed Al Sager
CURENT, Department of EECS
The University of Tennessee
Knoxville, TN, USA
malsager@vols.utk.edu

Dingrui Li
CURENT, Department of EECS
The University of Tennessee
Knoxville, TN, USA
dli35@vols.utk.edu

Leon M. Tolbert
CURENT, Department of EECS
The University of Tennessee
Knoxville, TN, USA
tolbert@utk.edu

Fred Wang
CURENT, Department of EECS
The University of Tennessee
Oak ridge National Laboratory
Knoxville, TN, USA
fred.wang@utk.edu

Hua Bai
CURENT, Department of EECS
The University of Tennessee
Knoxville, TN, USA
hbai2@utk.edu

***Abstract*—A hybrid microgrid is an attractive concept that aims to deliver energy to local ac and dc loads, reducing the strain imposed on the electrical grid. A hybrid microgrid of a flexible manufacturing plant consists of dc and ac loads, and distributed energy resources interfaces with the distributed grid through a power conditioning system to enable grid support capabilities and control power flow. To evaluate the controller functions of the hybrid microgrid, an appropriate testing platform is required. In this paper, the plant is emulated via a converter-based hardware testbed. The developed hardware testbed serves as a realistic model of the flexible manufacturing plant to test the controls and different scenarios to address potential issues or challenges with the control strategies and algorithms before system deployment. In addition, the hardware testbed provides the opportunity to validate the system's response under different operating conditions in a controlled environment, leading to a more robust and reliable system design.**

Keywords—Flexible hybrid microgrid, manufacturing plant, power conditioning system, converter-based hardware testbed

I. Introduction

According to the Department of Energy (DOE), 24% of the total energy was consumed by the manufacturing sector in the U.S in 2018. The core mission of the Advanced Manufacturing Office (AMO) of DOE is to improve the efficiency and reduce the energy consumption in industrial manufacturing [1]. With increasing demand for electronics and other high-tech loads that require dc power, the interest in dc microgrids (MGs) has grown. However, much of the existing infrastructure, including power generation and distribution, is based on ac, and this dominance is expected to continue for many decades to come. As a result, a hybrid MG combining dc and ac MGs may be the most realistic scenario [2]. In this approach, the appropriate sources, storage systems, and loads are distributed between the dc and ac sub-grids, allowing for efficient power conversion and distribution. Hence, a hybrid connection of ac and dc MGs is proposed, which can support the dc and ac loads simultaneously, and increase the grid resiliency [3]. To form a hybrid MG, power electronics-based power conditioning systems (PCSs) are needed. One example hybrid MG for a flexible manufacturing plant (FMP) is shown in Fig. 1, where a three-port converter serves as the interface of the ac and dc MGs. A hybrid MG usually requires a centralized MG controller to coordinate different components (sources, loads, etc.).

Testing is a critical step for MG controller implementation, requiring an appropriate platform. A hybrid MG contains multiple power electronic components. In digital simulation-based platforms, modeling detailed converter models will lead to heavy computation burden. Moreover, digital simulation platforms are unable to accurately represent system behavior when confronted with noise and numerical oscillations. This limitation persists unless highly intricate models are employed to precisely simulate each component, which further increases the system complexity. On the other hand, simplifying the converter model may also lead to inaccurate testing results.

To solve these issues, a converter-based emulation platform is developed in this paper, where the converters will emulate different system components and will be interconnected to demonstrate different power flow scenarios through the system. The advantages of deploying a converter based HTB include a more accurate depiction of system behavior, allows for real-time measurements and system control, and permits flexibility

in testing [4]. In the HTB, the central controller (CC) actively communicates with each of the local controllers (LCs) that are integrated within the converters in real-time to exchange data, evaluates the status of the different MG components, and executes system-level control. Evaluating a physical FMP system under various conditions (steady state, transition, fault, etc.) presents numerous challenges, including cost implications, reduced productivity caused by downtime, complexities associated with replicating faults that directly affect the grid, and the overall elevated risk of equipment damage.

The remaining sections of the paper are organized as follows: Section II outlines the FMP system architecture and design, Section III explores controller requirements and design, Section IV presents the experimental results, and Section V concludes the paper.

II. FMP System Architecture and Design

The example FMP system is illustrated in Fig. 1. The dc bus encompasses a 0.8 MW photovoltaic (PV) with a dc/dc converter, a 0.6 MW battery energy storage system (BESS) along with its respective dc/dc converter, and dc critical and non-critical loads of 0.4 MW. The ac plant has a similar configuration to the dc bus, however the PV and BESS interface with the ac bus through dc/ac inverters. Additionally, it includes a 1.2 MW generator; the generator's output power is deliberately selected to ensure the provision of backup power for the critical loads of the dc and ac sub-grids in scenarios where the other DER's outputs are zero and grid access is unavailable.

A. Power Conditioning System

The PCS interconnects the ac and dc buses with the medium voltage (MV) distribution grid and consists of three bidirectional power electronic converters. The converter-based PCS offers several benefits, such as the ability to smoothly transition between grid-connected and islanded mode by eliminating the need for resynchronization, reducing the impacts of unbalanced loads on the main grid through control techniques, providing isolation of faults; offering better system protection [5], and providing reactive power support to the distribution grid and the ac bus of the MG independently [6, 7]. However, PCSs have several disadvantages. These include the complexity arising from integrating multiple components and control algorithms, energy losses during power conversion in the power electronic-based converters, the need for robust protection mechanisms to mitigate faults, overloads, and voltage fluctuations [8, 9]. Moreover, PCSs depend on sophisticated control systems and delicate electronic components, increasing the risk of failures, necessitating frequent maintenance, and potentially impacting the overall system reliability. The need for incorporating power conversion systems to address these issues and offer optimized performance, reliability, functionality, and reduced cost is a high priority [10].

B. FMP System Loads

The loads of the system are categorized as critical and non-critical loads. The critical load represents the necessary power needed to support certain functions of the system to avoid life threatening circumstances, system crashes, or any other essential services that must remain operational. On the other hand, the non-critical load may briefly be shut off without inflicting any damage to the system or associated manufacturing line or products.

C. Operation Modes

The hybrid MG operates in two distinct modes: grid connected mode and islanded mode.

1) Grid-connected mode: The MV distribution grid ensures a consistent voltage and frequency, providing reliable support to all loads on the ac and dc bus. In cases where the DERs are unable to fully support the loads on both buses, the grid steps in to supply the remaining power. Furthermore, the MG can offer active power grid support by adjusting the output of the DERs. It reduces the DERs' output when the grid needs to release active power and increases it when the distribution grid needs to absorb active power.

2) Islanded mode: the hybrid MG operates independently from the distribution grid. If the energy produced by the DERs

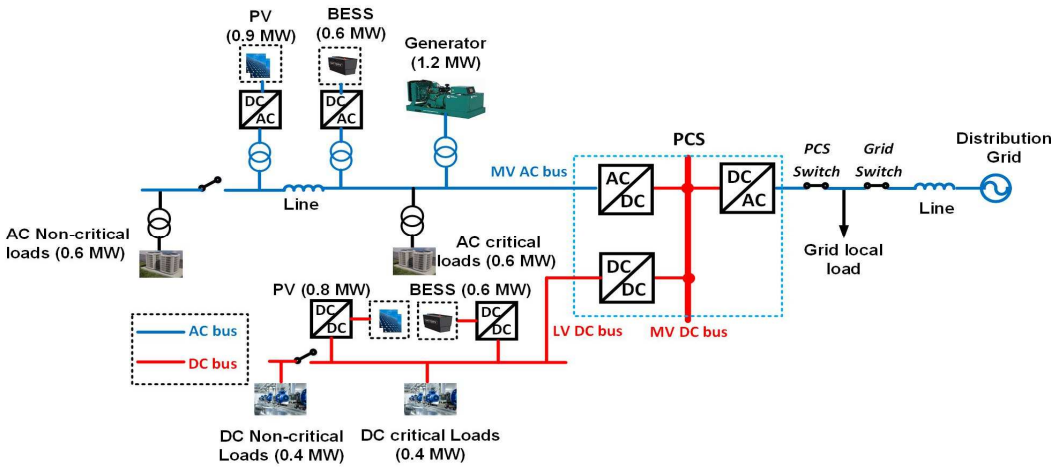

Fig. 1. Example FMP system.

is insufficient to meet the total load, the CC will prioritize critical loads by turning off non-critical loads. On the other hand, during periods of high solar irradiance, when the DERs can adequately meet the MG's load demand, any surplus power can be utilized to support the local load of the grid, which includes both three-phase balanced loads.

D. FMP System Requirements

The FMP is required to establish constant communication with the grid, providing updates on the system's component status. It should also ensure steady-state operation in both grid-connected and islanded modes, facilitating seamless transitions between the two. It is crucial to always ensure uninterrupted support for critical loads. However, during islanding mode, if the output from DERs falls short, non-critical loads should be shed to prioritize the critical ones. Additionally, the system should offer grid support during grid-connection by actively providing or absorbing power. To promote battery health and ensure optimal operation, continuous monitoring of the state of charge (SOC) and effective management of BESS charging are essential. The developed HTB should have the capability to model the FMP structure while successfully meeting the system requirements.

III. Hardware Testbed Design

A. HTB System Architecture

Fig. 2 illustrates the HTB architecture depicting the emulation of the example FMP system. The architecture consists of six two-level, three-phase converters. The grid emulator (C1), dc plant emulator, ac plant emulator, and PCS emulators (C2, C3, and C5) are key components. Converter C6 is responsible for emulating the dc plant, comprising the DERs and loads. Similarly, converter C4 emulates the ac plant, incorporating loads and DERs including a generator. Despite being a three-phase converter, C6 is configured as three separate dc/dc converters to accurately emulate the PV, BESS, and critical/noncritical loads as in [11]. A dc power supply establishes the dc link and provides power to compensate for system losses due to the circulating loop FMP configuration.

B. Communication

The green lines in Fig. 2 represent the CAN-bus communication, enabling data exchange between the LCs on each converter and the CC. The LC controllers use the TMS320 DSP from TI, while the central controller is the CompactRIO from National Instrument (NI). Through the CAN-bus, the LCs and CC can seamlessly transmit and receive data, enabling effective coordination and control within the system.

C. Physical HTB

The physical HTB has been built in the lab, as shown in Fig. 3, using six converters based on the design architecture. Table I shows the system ratings of the HTB.

TABLE I. HTB System Ratings

HTB component	Power input	Voltage input	Current input
Grid Emulator C1	2250 W	150 V dc	15 A
Grid PCS C2	1500 VA	75 V ac	20 A
Plant PCS C3	2250 W	150 V dc	15 A
AC Plant C4	1500 VA	75 V ac	20 A
DC PCS C5	2250 W	150 V dc	15 A
DC Plant C6	750 VA	75 V dc (each branch)	10 A (each branch)

IV. Controller Functions

Both the CC and LC have unique responsibilities and independent control mechanisms that operate based on the exchanged information. This section presents a detailed

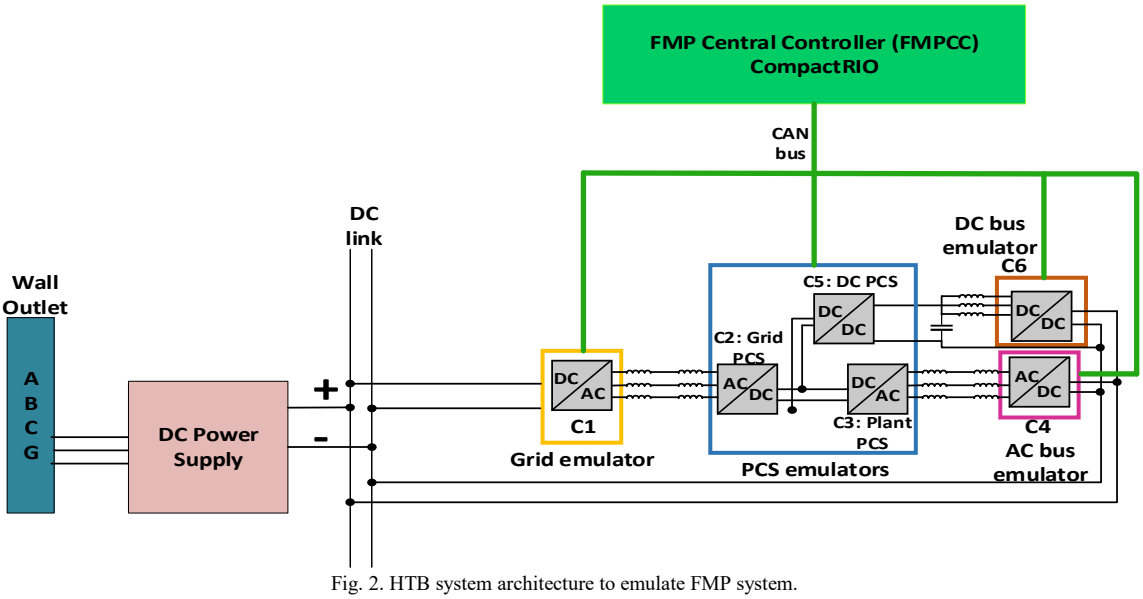

Fig. 2. HTB system architecture to emulate FMP system.

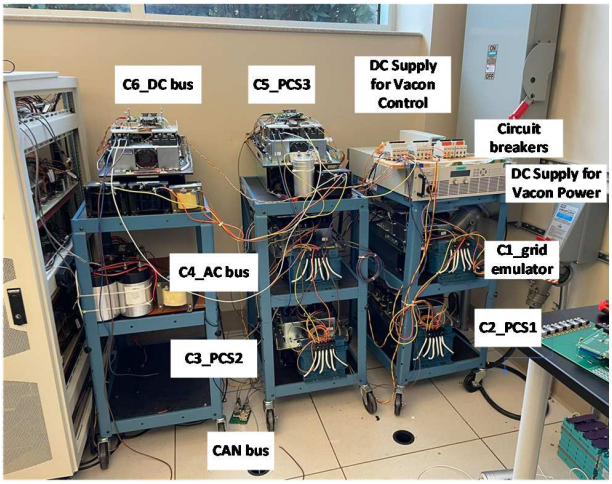

Fig. 3. Hardware testbed.

description of the control strategies employed in the CC and LCs.

A. Local Controllers

The LCs on each HTB emulator consistently exchange real-time data with the CC, including operation mode, voltage, power, and frequency. This facilitates the central controller in issuing commands and making decisions based on system information. Furthermore, the LCs employ diverse control strategies depending on the operational mode, such as fault, grid-connected, and islanded modes. Table II provides a description of the control functions employed for each of the emulators.

TABLE II. LOCAL CONTROLLER FUNCTIONS

Emulator	Grid-connected mode	Islanded mode
C1- grid emulator	Grid-emulator	Local load emulator
C2- Grid PCS	Grid-following	Grid-forming if excess power of DERs is fed to grid local load, otherwise it is disabled.
C3- Plant PCS	Grid-forming	Grid-following
C4- ac bus	Grid-following SOC calculation	Grid-forming SOC calculation
C5- dc PCS	Regulate LV dc	Regulate LV dc
C6- dc bus	Power regulation SOC calculation	Power regulation SOC calculation

In grid-connected mode, the grid emulator C1 effectively emulates the grid by providing a stable ac voltage source. In islanded mode, it functions as a local load for the grid and can accept surplus power from the MG during high PV output periods. The grid-side PCS C2 acts as a grid-forming unit during grid-connected operation and as a grid-following unit during islanded operation. On the other hand, the ac plant-side PCS C3 operates in grid-forming mode during grid-connected operation and switches to grid-following mode in islanded operation. The ac plant emulator C4 tracks the SOC of the BESS while operating in grid-following mode during grid-connected operation. In islanded mode, it takes on the responsibility of establishing and maintaining the voltage and frequency using the BESS, functioning in grid-forming mode. The dc PCS C5 is responsible for regulating the low dc voltage. Meanwhile, the dc plant emulator C6 monitors the SOC in both grid-connected and islanded modes and regulates the power.

B. Central Controller

The central controller has several main functions, including the implementation of a Finite State Machine (FSM), PQ control, and SOC control.

1) Finite-State-Machine: The Finite State Machine enables the central controller to transition between different operational states based on predefined conditions and events. By employing a FSM, the central controller can effectively manage and coordinate various system operations, such as startup, shutdown, fault detection, and transition between grid-connected and islanded modes as shown in Fig. 4. A brief description of the different operational states is provided below.

a) Shutdown: In this state, the entire FMP system is deactivated and shut down.

b) Ready-to-run: The system is powered on and operational, but there is no active power flow within the system.

c) Grid-connected: The FMP system is connected to the grid, and power exchange between the system and the grid is established.

d) Islanded: In this state, the FMP system operates in an isolated mode, disconnected from the grid, and relies solely on its own energy resources.

e) Fault detection: The FSM transitions to this state when a fault or abnormal condition is detected within the system. It triggers specific protection mechanisms and initiates corrective actions to mitigate the fault and restore normal operation.

2) PQ control: Plays a vital role in ensuring the power quality of the system. The central controller utilizes PQ control algorithms to regulate and maintain the desired levels of active power and reactive power exchanged in accordance with the

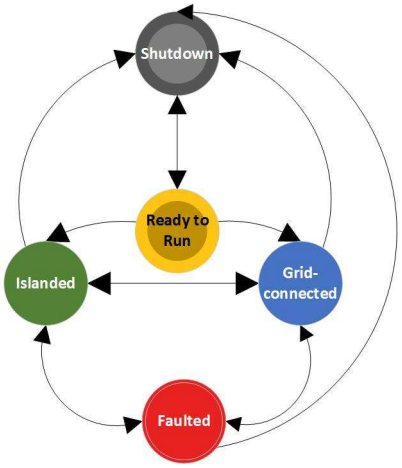

Fig. 4. FSM modes of HTB control.

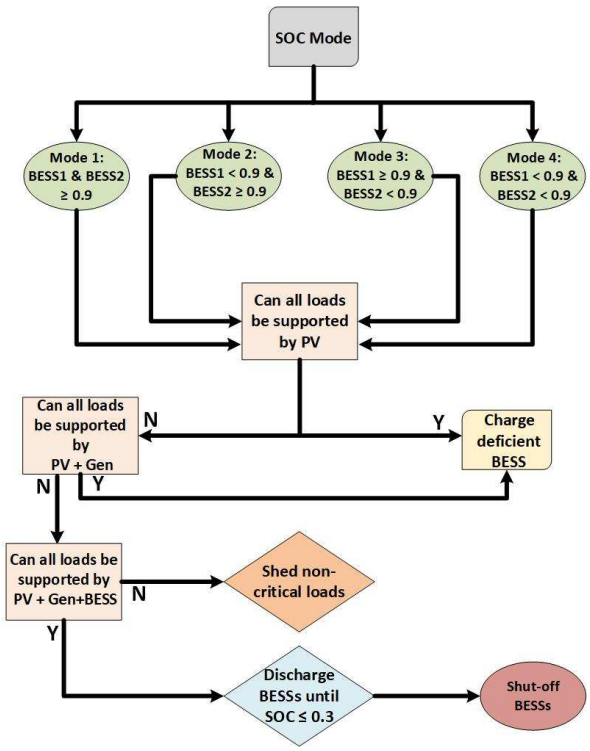

Fig. 5 State of charge algorithm diagram.

assigned references [12]. Table III showcases the PQ control functions of the HTB in grid-connected mode and islanded mode for various scenarios.

TABLE III. PQ CONTROL FUNCTIONS

Scenario	PQ control function in grid-connected mode	PQ control function in islanded mode
Active power support Excess Power of DERs	• Limit active power from grid. • Charge BESSs. • Support grid local load.	• Charge BESSs. • Support grid local load.
Insufficient power of DERs	• Active power injection from the grid.	• Load shedding to prioritize critical loads.
Grid support	• Active power injection to the grid. • Active power absorption from the grid.	• N/A
Grid fault ride-through	• Adjust active power to mitigate voltage balance/unbalance faults.	• N/A
Reactive power support	• Grid-side PCS C1 provides reactive power compensation to the grid. • Plant-side PCS C5 provides reactive power compensation to the ac bus.	• Grid-side PCS C1 provides reactive power compensation to the grid. • Plant-side PCS C5 provides reactive power compensation to the ac bus.

3) SOC control

Additionally, the central controller is responsible for SOC control, which involves monitoring and managing the charge of the BESSs by employing equation (1), as discussed in [13]:

$$SOC_t = SOC_{t-1} - \int_0^t \frac{I(t)}{C_0} dt \quad (1)$$

where SOC_t and SOC_{t-1} denote the current and previous state of charge value respectively. $I(t)$ denotes the charge/discharge current, and C_0 denotes the battery capacity.

By implementing the SOC control algorithm as shown in Fig. 5, the central controller optimizes the charging and discharging of the energy storage systems, ensuring their efficient utilization, and prolonging their lifespan. Based on the developed SOC control strategy, when there is a high PV power output and both critical and non-critical loads are adequately supported, any excess power generated by the DER is utilized to charge the depleted BESS. The charging process continues until the BESS reaches a SOC of 90%. On the contrary, when there is insufficient PV power to meet the demand of critical and non-critical loads, the BESS discharges its stored energy [14]. The discharge process continues until the SOC of the BESS reaches 30%. Once the SOC reaches this threshold, the BESS is shut down to prevent further depletion of its energy reserves.

The ideal SOC limits of a BESS can vary depending on various factors such as the specific battery chemistry, manufacturer recommendations, and operational requirements. However, in general, it is common to consider SOC limits between 30% and 90%. This range helps to maximize the battery's lifespan, efficiency, and performance while allowing for a reasonable energy storage capacity during charging and discharging operations. The precise SOC limits may differ based on the specific application and requirements of the BESS. This enables effective management of energy storage resources and enhances the overall performance and reliability of the system.

V. EXPERIMENTAL RESULTS

Experiments are performed to validate the ability of the HTB to emulate the FMP system and the implemented control algorithms by capturing real-time measurements. The tested controller functions encompass a range of important aspects including grid transitions, PQ controller, SOC controller, and grid support. These functions are thoroughly evaluated to assess their effectiveness and performance within the system.

A. FSM Control Verification

The steady-state operations and mode transitions of the FMP system are governed by the FSM control algorithm. Fig. 6 to Fig. 9 showcase various scenarios, including steady-state grid-connected mode, islanded mode, grid reconnection, planned islanding, and black start capability.

In Fig. 6, it is evident that the MV dc link, low dc bus voltage, and ac bus voltage have all been established, allowing the grid-side PCS to enable current flow from the grid and partially support the system load. In Fig. 7, the grid-side PCS is deactivated, resulting in no power exchange with the distribution grid. This leads to the system operating in islanded mode, with the DER sources taking over the responsibility of sustaining the system loads. However, in some cases, the grid-side PCS can be reactivated during islanded mode if the DER sources can fully supply the system load, charge the BESSs,

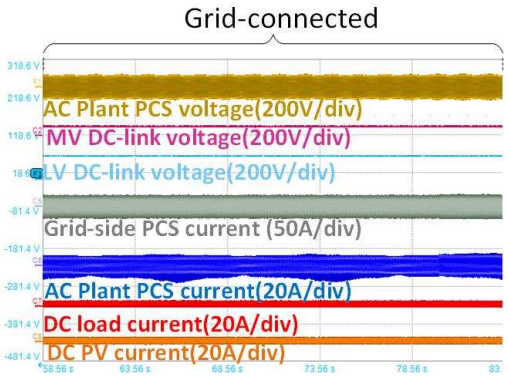

Fig. 6. Steady-state waveforms for grid-connected MG.

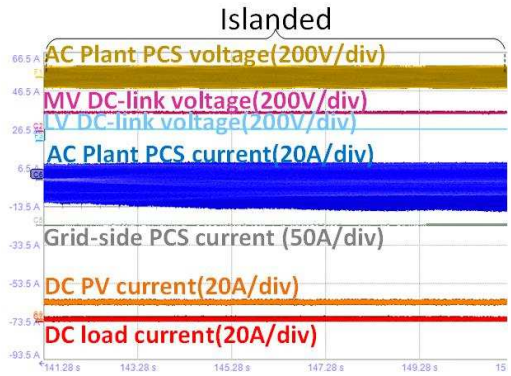

Fig. 7. Steady-state waveforms for islanded MG.

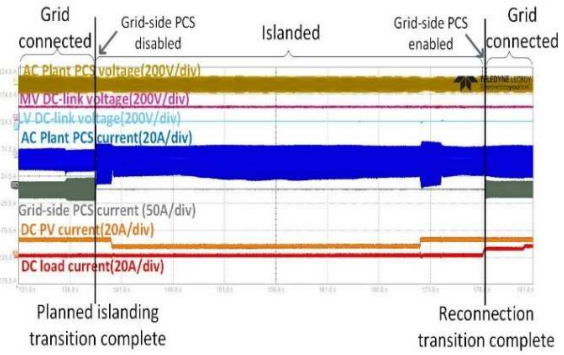

Fig. 8. Planned islanding and reconnection transition waveforms.

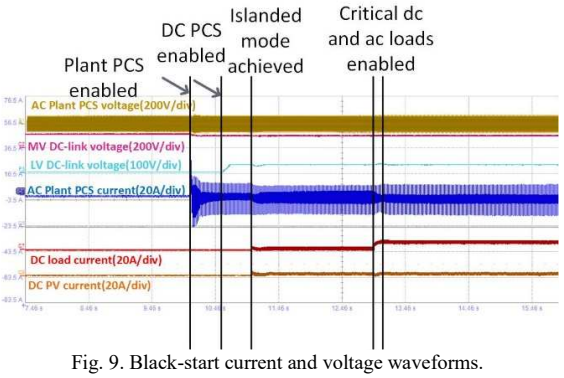

Fig. 9. Black-start current and voltage waveforms.

and support the grid local load. Fig. 8 illustrates the transition from grid-connected to islanded mode (planned-islanding) and then back to grid-connected mode (reconnection), with the grid-side PCS being disabled during the islanding operation. Fig. 9 illustrates the black-start waveform. While the IEEE 2030.7 standard [15] does not provide a specific definition for black-start transitions in MG controllers due to the unique nature of each system, our approach involves transitioning the system to islanding mode before transitioning to grid-connected mode once it is turned on and in standby mode similar to [16].

B. PQ Control Verification

During steady-state operation, the PQ controller needs to be adaptable and responsive to the system conditions, as indicated in Table III. These scenarios are thoroughly tested to validate the performance and effectiveness of the PQ controller.

In Fig. 10, the system operates in islanded mode from $t_0$to t_1, providing support to both critical and non-critical loads. At t_1, the PV output on the ac bus decreases, resulting in the shedding of non-critical loads. From t_2 to t_3, the PV output increases, allowing the non-critical loads to be supported once again. At t_4, the PV output on both the dc and ac bus increases, and shortly after, the grid-side load is taken up. At t_5, as the PV output decreases, the local grid load is disconnected to ensure the microgrid provides full support to its ac and dc loads.

In Fig. 11, the system operates in grid-connected mode, with all loads supported by the DERs and the distribution grid. At t_1, the PV output on the ac bus increases, leading to reduced power consumption from the grid. Conversely, at t_2, the PV output on the ac bus decreases, resulting in increased power consumption from the grid. The outcomes depicted in Fig. 10 and Fig. 11 confirm the validity of the PQ control and the operation of the FMP system using the HTB setup.

C. SOC Control Verification

The screenshot in Fig. 12 displays the Human-Machine Interface (HMI) of the HTB system. It is evident from the image that the system is currently operating in islanded mode. The BESSs are shown to be charging, and the grid local load is being supported (highlighted within white dashed rectangles). The arrows depicted in the image indicate the direction of power flow within the system. Furthermore, the graph in the bottom right corner indicates that BESS1 and BESS2 are consuming active power.

VI. Conclusions

This paper presented a comprehensive study on a hybrid MG for a flexible manufacturing plant using a converter-based hardware testbed. The developed HTB serves as a realistic model of the FMP, allowing for testing of controls and different scenarios before system deployment. The HTB provides an opportunity to validate the system's response under various operating conditions in a controlled environment, leading to a more robust and reliable system design and system performance of the hybrid MG. The findings from this study contribute to the development of more reliable and efficient hybrid MG systems, which can reduce strain on the electrical grid and improve energy delivery to local ac and dc loads in manufacturing plant

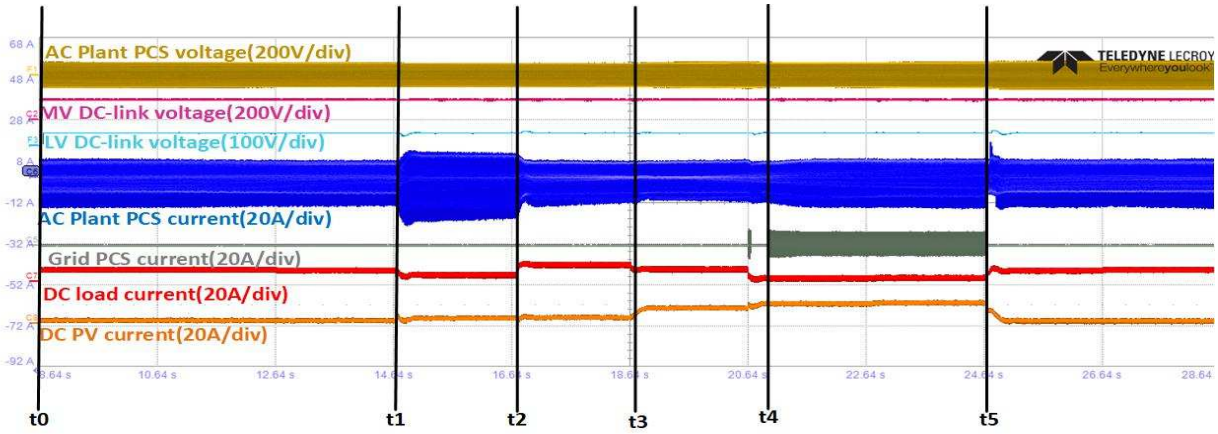

Fig. 10. Islanded mode operation: Dynamic waveform illustrating load shedding and DERs power output fluctuations.

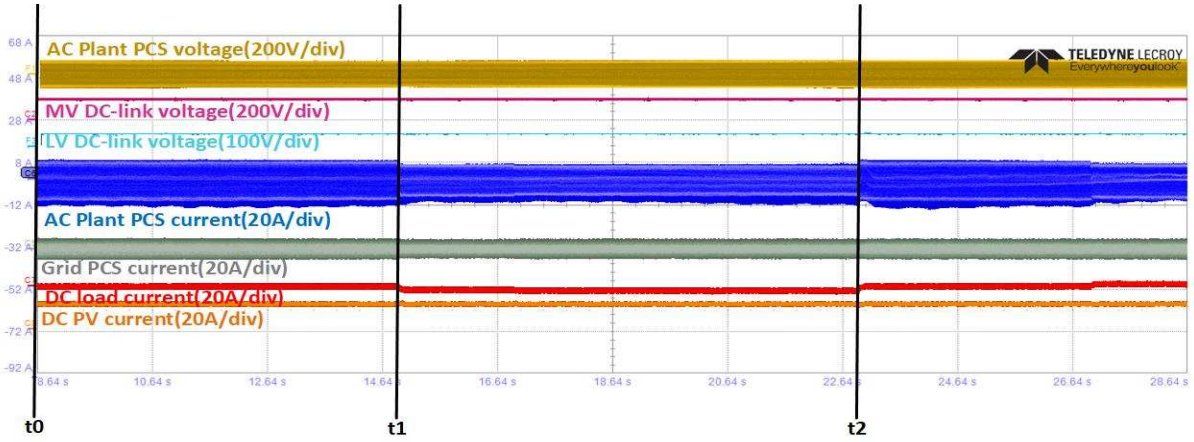

Fig. 11. Grid-connected mode operation: Dynamic waveform illustrating load shedding and DERs power output fluctuations.

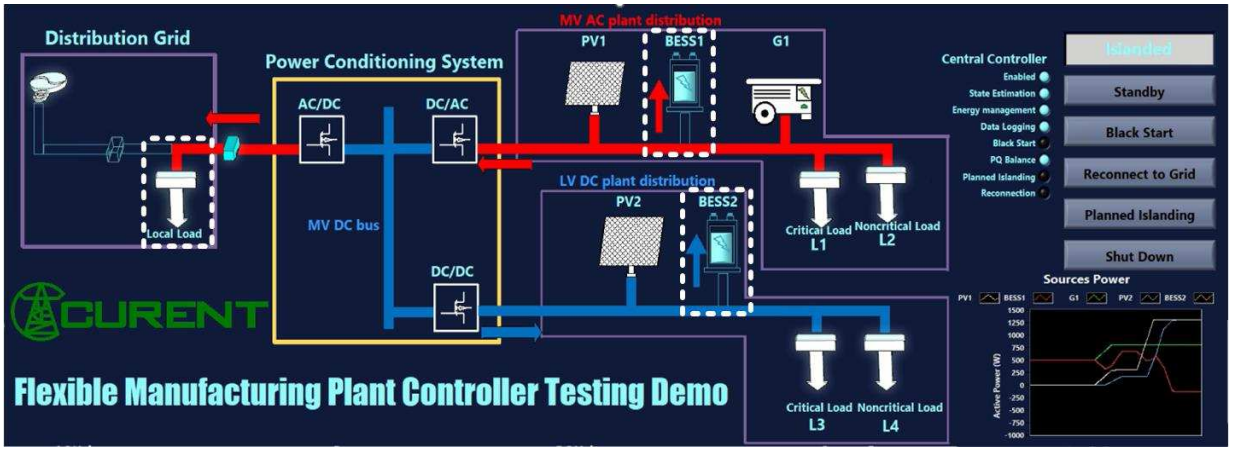

Fig. 12. Human-machine-interface indicating BESS charging during high PV output.

The FMP system architecture and design were discussed, including the PCS that interconnects the ac and dc buses with the distribution grid. The steady-state operation modes and transitions of the hybrid MG were explained, along with the roles of the LCs and central controller CC in each mode.

Experimental results from the HTB setup were presented to verify the implemented control algorithms and evaluate the system's performance. The FSM control algorithm demonstrated successful mode transitions and steady-state operation. The PQ controller effectively managed active power exchange with the grid in different scenarios, while the SOC control algorithm optimized the charging and discharging of the BESSs. Overall, the use of the converter-based HTB proved to

be a valuable tool for emulating the FMP system and testing and validating the control strategies.

Future research could prioritize fine-tuning control strategies and exploring various scenarios, including grid mode transitions and steady-state operation with the presence of a PCS. Additionally, implementing fault ride-through capabilities and response control mechanisms can further enhance the overall performance and resilience of the hybrid MG system.

ACKNOWLEDGEMENT

This work was primarily funded by the Advanced Manufacturing Office (AMO), U.S. DOE under Award Number DE-EE0009134. This work made use of the Engineering Research Center Shared Facilities supported by the Engineering Research Center Program of the National Science Foundation and DOE under NSF Award Number EEC-1041877 and the CURENT Industry Partnership Program.

REFERENCES

[1] "Analysis finds decrease in U.S. manufacturing energy consumption, " U.S. Department of Energy. https://www.energy.gov/eere/amo/articles/analysis-finds-decrease-us-manufacturing-energy-consumption (accessed Feb. 6 2023).

[2] P. C. Loh, D. Li, Y. K. Chai, and F. Blaabjerg, "Autonomous operation of hybrid microgrid with ac and dc subgrids," *IEEE Transactions on Power Electronics,* vol. 28, no. 5, pp. 2214-2223, May 2013.

[3] R. Majumder, "A hybrid microgrid with dc connection at back to back converters," *IEEE Transactions on Smart Grid,* vol. 5, no. 1, pp. 251-259, Jan. 2014

[4] D. Li, Y. Ma, C. Zhang, H. Yin, I. Ray, Y. Su, *et al.*, "Development of a converter based microgrid test platform," in *Proc. IEEE Energy Conversion Congress and Exposition (ECCE)*, 2019, pp. 6294-6300.

[5] R. Chen, F. Wang, L. M. Tolbert, X. Huang, D. Li, C. Nie, *et al.*, "10 kV SiC MOSFET based medium voltage power conditioning system for asynchronous microgrids," *IEEE Access,* vol. 10, pp. 73294-73308, Jul. 2022.

[6] X. Zhu, A. Singh, and B. Mather, "Grid value investigation of medium-voltage back-to-back converters," in *Proc. IEEE Power & Energy Society Innovative Smart Grid Technologies Conference (ISGT)*, Feb. 2021, pp. 1-5.

[7] N. M. Salgado-Herrera, A. Medina-Ríos, R. Tapia-Sánchez, and O. Anaya-Lara, "Reactive power compensation through active back to back converter in type-4 wind turbine," in *Proc. IEEE International Autumn Meeting on Power, Electronics and Computing (ROPEC)*, Nov. 2016, pp. 1-6.

[8] M. Najafzadeh, R. Ahmadiahangar, O. Husev, I. Roasto, T. Jalakas, and A. Blinov, "Recent contributions, future prospects and limitations of interlinking converter control in hybrid ac/dc microgrids," *IEEE Access,* vol. 9, pp. 7960-7984, Jan. 2021.

[9] F. S. Oliveira, L. F. Encarnação, R. S. Camargo, and E. J. B. Peña, "Multilevel back-to-back cascaded h-bridge converter with model predictive control," in *Proc. IEEE Industrial Electronics Society (IECON)*, Oct. 2019, pp. 1880-1885.

[10] X. Zhu, A. Singh, and B. Mather, "Grid value analysis of medium-voltage back-to-back converter on der hosting enhancement," *IEEE Transactions on Power Delivery,* vol. 38, no. 1, pp. 553-563, Feb. 2023.

[11] H. Li, D. Li, Z. Gao, Y. Ma, Z. Yang, F. Wang, *et al.*, "Development of a power electronics-based testbed for a flexible combined heat and power system," in *Proc. IEEE Energy Conversion Congress and Exposition (ECCE)*, Oct. 2021, pp. 764-770.

[12] W. Bai and K. Lee, "Distributed generation system control strategies in microgrid operation," in *Proc. Proceedings Volumes,* vol. 47, no. 3, pp. 11938-11943, Jan. 2014.

[13] L. Castañer and S. Silvestre, "Introduction to Photovoltaic Systems and PSpice, " 2006, pp. 1-18.

[14] D. Li, Y. Ma, C. Zhang, H. Yin, Y. Su, L. Zhu, *et al.*, "A converter-based battery energy storage system emulator for the controller testing of a microgrid with dynamic boundaries and multiple source locations," in *Proc. IEEE Energy Conversion Congress and Exposition (ECCE)*, Oct. 2022, pp. 1-8.

[15] "IEEE Standard for the Specification of Microgrid Controllers," *IEEE Std 2030.7-2017,* pp. 1-43, 2018.

[16] J. Wang, A. Pratt, and M. Baggu, "Design of a state machine for smooth microgrid transition operation," in *Proc. IEEE Power & Energy Society Innovative Smart Grid Technologies Conference (ISGT)*, Feb. 2018, pp. 1-5.